

Project Report

Dyadic Helmholtz Green's Function for Electromagnetic Wave Transmission/Diffraction through a Subwavelength Nano-Hole in a 2D Quantum Plasmonic Layer: An Exact Solution Using "Contact Potential"-like Dirac Delta Functions

Désiré Miessein ^{1,2} , Norman J. M. Horing ^{2,*} and Harry Lenzing ²

¹ Department of Physics and Engineering Physics, Fordham University, Bronx, NY 10458, USA; dmiessein@fordham.edu

² Department of Physics, Stevens Institute of Technology, Hoboken, NJ 07030, USA; harry07757@comcast.net

* Correspondence: nhoring@stevens.edu

Abstract: The dyadic Helmholtz Green's function for electromagnetic (EM) wave transmission/diffraction through a subwavelength nano-hole in a two-dimensional (2D) plasmonic layer is discussed here analytically and numerically, employing "contact potential"-like Dirac delta functions in 1 and 2 dimensions ($\delta(z)$ and $\delta(x)\delta(y) \equiv \delta^{(2)}(\vec{r})$). This analysis is carried out employing a succession of two coupled integral equations. The first integral equation determines the dyadic electromagnetic Green's function \hat{G}_{fs} for the full non-perforated 2D quantum plasma layer in terms of the bulk 3D infinite-space dyadic electromagnetic Green's function \hat{G}_{3D} , with $\delta(z)$ representing the confinement of finite quantum plasma conductivity to the plane of the plasma layer at $z = 0$. The second integral equation determines the dyadic electromagnetic "hole" Green's function \hat{G}_{hole} for the perforated 2D quantum plasma layer (containing the nano-hole) in terms of the dyadic electromagnetic Green's function \hat{G}_{fs} for the full non-perforated 2D plasma layer, with $\delta^{(2)}(\vec{r})$ describing the exclusion of the quantum plasma layer conductivity properties from the nano-hole region in the vicinity of $\vec{r} = 0$ on the plane. Taking the radius of the subwavelength nano-hole to be the smallest length scale of the system in conjunction with the 2D Dirac delta function representation of the excluded nano-hole plasma conductivity, both of the successive coupled integral equations are solved *exactly*, and we present a thorough numerical analysis (based on the exact analytic solution) for the resulting dyadic "hole" Green's function \hat{G}_{hole} in full detail in both 3D and density plots. This result has been successfully applied to the determination of electromagnetic wave transmission/diffraction through the nano-hole of the perforated quantum plasmonic layer, jointly with the EM wave transmission through the rest of the plasma layer. This success necessarily involves spatial translational asymmetry induced by the use of spatial Dirac delta functions confining finite conductivity to the 2D quantum plasma sheet and the excision at a bit of it about the origin to represent the nano-hole perforation, thus breaking spatial translational invariance symmetry.

Keywords: Green's function; electromagnetic wave transmission/diffraction; Helmholtz; nano-hole; plasmonic layer; subwavelength; contact potential; dirac delta function; dyadic



Citation: Miessein, D.; Horing, N.J.M.; Lenzing, H. Dyadic Helmholtz Green's Function for Electromagnetic Wave Transmission/Diffraction through a Subwavelength Nano-Hole in a 2D Quantum Plasmonic Layer: An Exact Solution Using "Contact Potential"-like Dirac Delta Functions. *Symmetry* **2022**, *14*, 1134. <https://doi.org/10.3390/sym14061134>

Academic Editors: Fabio Rinaldi, Silvestro Fassari and Young S. Kim

Received: 23 January 2022

Accepted: 26 May 2022

Published: 31 May 2022

Publisher's Note: MDPI stays neutral with regard to jurisdictional claims in published maps and institutional affiliations.



Copyright: © 2022 by the authors. Licensee MDPI, Basel, Switzerland. This article is an open access article distributed under the terms and conditions of the Creative Commons Attribution (CC BY) license (<https://creativecommons.org/licenses/by/4.0/>).

1. Introduction

The transmission/diffraction properties of an electromagnetic dyadic Green's function for wave propagation through a nano-hole in a two-dimensional (2D) quantum plasmonic layer are analyzed here using a succession of two coupled integral equations jointly with "contact interaction"-like Dirac delta functions representing positional localization of the layer and the nano-hole [1–3]. The nano-hole is taken to lie on a 2D plasmonic sheet (located on the plane $z = 0$ embedded in a three-dimensional (3D) bulk host medium with background dielectric constant $\epsilon_b^{(3D)}$). In Section 2 of this paper, we briefly review in some

detail the analytic determination of the electromagnetic dyadic Helmholtz Green's function \widehat{G}_{fs} in the presence of the layer in which a uniform two-dimensional quantum plasma is embedded. The first associated integral equation employs a "contact interaction"-like 1D Dirac delta function that localizes the plasma conductivity to the 2D sheet at $z = 0$ and its solution yields \widehat{G}_{fs} in terms of the well-known bulk 3D infinite-space electromagnetic dyadic Green's function \widehat{G}_{3D} explicitly. Section 3 reviews the electromagnetic dyadic Helmholtz Green's function solution \widehat{G}_{hole} for the perforated 2D plasmonic layer embedded in a 3D host medium, with the presence of a nano-hole aperture in the subwavelength regime. In this second associated integral equation, the excision of nano-hole conductivity from the 2D plasma sheet is represented in terms of a "contact interaction"-like 2D Dirac delta function; the exact solution of this second integral equation yields \widehat{G}_{hole} in terms of \widehat{G}_{fs} explicitly, which has been determined as above in terms of \widehat{G}_{3D} . The results of our thorough numerical analysis (based on the exact analytic solution) for the perforated plasma layer electromagnetic dyadic Helmholtz Green's function are exhibited in Section 4 with illustrative 3D and density plots showing results in the near-, middle- and far-field zones of the transmission region. Finally, our conclusions are summarized in Section 5. Obtaining an exact analytic solution to the involved electromagnetic issues of diffraction jointly with transmission through the 2D plasma sheet has necessarily introduced spatial translational asymmetry through the use of spatial Dirac delta functions confining finite conductivity to the plasma sheet and the excision of a bit of it about the origin to represent the nano-hole perforation.

2. Dyadic Electromagnetic Green's Function for a Full 2D Plasmonic Layer Embedded in a 3D Bulk Host Medium

Integral Equation for the Full 2D Plasma Layer Electromagnetic Dyadic Helmholtz Green's Function $\widehat{G}_{fs}(\vec{k}_{\parallel}; z, z'; \omega)$ and Solution

We consider a two-dimensional quantum plasmonic layer S_1 with a dynamic, nonlocal 2D plasma conductivity, $\sigma_{fs}^{(2D)}(\vec{k}_{\parallel}, \omega)$, located on the plane $z = 0$, embedded in a three-dimensional infinite bulk host medium with background dielectric constant $\epsilon_b^{(3D)}$ (Figure 1). The associated electromagnetic dyadic Helmholtz Green's function including the full two-dimensional plasmonic sheet, \widehat{G}_{fs} without a nano-hole, satisfies the integral equation (position/frequency representation) [1–3]

$$\begin{aligned} \widehat{G}_{fs}(\vec{r}, \vec{r}'; \omega) &= \widehat{G}_{3D}(\vec{r}, \vec{r}'; \omega) \\ &+ \frac{4\pi i\omega}{c^2} \int d^3\vec{r}'' \int d^3\vec{r}''' \widehat{G}_{3D}(\vec{r}, \vec{r}''; \omega) \widehat{\sigma}_{fs}^{(2D)}(\vec{r}'', \vec{r}'''; \omega) \widehat{G}_{fs}(\vec{r}''', \vec{r}'; \omega), \end{aligned} \quad (1)$$

where \widehat{G}_{3D} satisfies the inversion condition

$$\left[\widehat{I} \left(\nabla^2 + \frac{\omega^2}{c^2} \epsilon_b^{(3D)} \right) - \nabla \nabla \right] \widehat{G}_{3D}(\vec{r}, \vec{r}'; \omega) = -\widehat{I} \delta^{(3D)}(\vec{r} - \vec{r}'), \quad (2)$$

as the bulk 3D infinite-space dyadic electromagnetic Green's function, and $\widehat{I} = \widehat{x}\widehat{x} + \widehat{y}\widehat{y} + \widehat{z}\widehat{z}$ is the 3D unit dyadic tensor and c is the speed of light in vacuum. The conductivity $\sigma_{fs}^{(2D)}$ of the full 2D plasmonic layer has the form

$$\widehat{\sigma}_{fs}^{(2D)}(\vec{r}, \vec{r}'; \omega) = \widehat{I} \sigma_{fs}^{(2D)}(\vec{r}_{\parallel}, \vec{r}'_{\parallel}; \omega) \delta(z) \delta(z'), \quad (3)$$

where $\vec{r} = (\vec{r}_{\parallel}; z)$ and $\widehat{\sigma}_{fs}^{(2D)}(\vec{r}_{\parallel}, \vec{r}'_{\parallel}; \omega)$ is the 2D plasmonic conductivity of the 2D sheet; $\delta(z)$ is the "contact potential"-like Dirac delta function employed to confine the conductivity to the plane of the 2D layer at $z = 0$. Fourier transforming $\vec{r}_{\parallel} - \vec{r}'_{\parallel} \mapsto \vec{k}_{\parallel} = k_x \widehat{e}_x + k_y \widehat{e}_y$ to lateral wavenumber representation,

$$\hat{\sigma}_{fs}^{(2D)}(\vec{k}_{\parallel}; z'', z'''; \omega) = \hat{I} \sigma_{fs}^{(2D)}(\vec{k}_{\parallel}; \omega) \delta(z'') \delta(z'''), \quad (4)$$

where $\hat{\sigma}_{fs}^{(2D)}$ is taken in the local limit as

$$\sigma_{fs}^{(2D)}(\vec{k}_{\parallel}; \omega) = \frac{i\omega}{4\pi} [\epsilon_b^{(3D)} - \epsilon(\omega)] d, \quad (5)$$

with $\epsilon(\omega)$ as the local, dynamic dielectric function of the 2D plasmonic layer of thickness d . It should be noted that 2D plasma nonlocality could easily be included here.

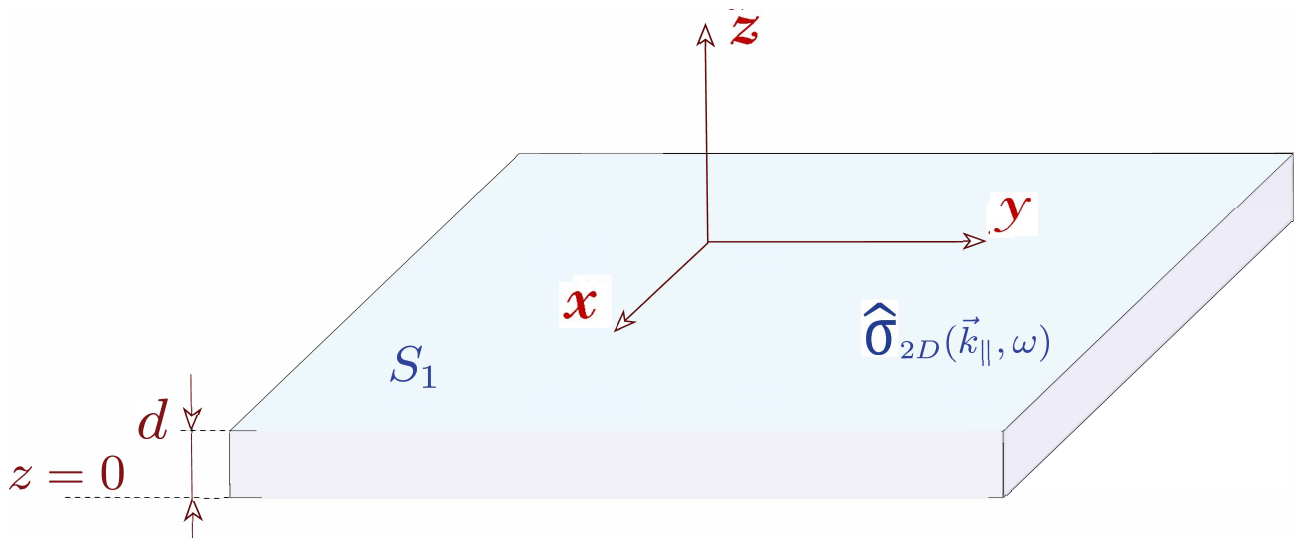


Figure 1. (Color online). Schematic illustration of a two-dimensional plasmonic layer S_1 of thickness d embedded at $z = 0$ in a three-dimensional bulk medium with dielectric constant $\epsilon_b^{(3D)}$.

The solution of Equation (1) for $\hat{G}_{fs}(\vec{k}_{\parallel}; z, z'; \omega)$ in \vec{k}_{\parallel} representation may be determined algebraically in terms of \hat{G}_{3D} by using Equation (4) in the indicated integrations of Equation (1), with the result [1–3]

$$\begin{aligned} \hat{G}_{fs}(\vec{k}_{\parallel}; z, z'; \omega) &= \hat{G}_{3D}(\vec{k}_{\parallel}; z, z'; \omega) \\ &+ \gamma \hat{G}_{3D}(\vec{k}_{\parallel}; z, 0; \omega) \\ &\times \left[\hat{I} - \gamma \hat{G}_{3D}(\vec{k}_{\parallel}; 0, 0; \omega) \right]^{-1} \hat{G}_{3D}(\vec{k}_{\parallel}; 0, z'; \omega), \end{aligned} \quad (6)$$

where we have defined γ as

$$\gamma = \frac{4\pi i \omega}{c^2} \sigma_{fs}^{(2D)}(\vec{k}_{\parallel}; \omega) \quad (7)$$

and the bulk 3D infinite-space dyadic electromagnetic Green's function \hat{G}_{3D} is

$$\begin{aligned} \hat{G}_{3D}(\vec{k}_{\parallel}; z, z'; \omega) &= -\frac{e^{ik_z|z-z'|}}{2ik_z} \\ &\times \left\{ \hat{I} - \frac{1}{q_\omega^2} \left[\vec{k}_{\parallel} \vec{k}_{\parallel} + k_z \operatorname{sgn}(z-z') (\vec{k}_{\parallel} \hat{e}_z + \hat{e}_z \vec{k}_{\parallel}) + \hat{e}_z \hat{e}_z (k_z^2 - 2ik_z \delta(z-z')) \right] \right\}, \end{aligned} \quad (8)$$

in mixed $(\vec{k}_{\parallel}; z, z')$ Fourier representation and $q_\omega = (\omega/c) \sqrt{\epsilon_b^{(3D)}}$. Furthermore,

$$k_z = \sqrt{q_\omega^2 - k_{\parallel}^2} \quad (9)$$

and

$$\text{sgn}(\bar{z}) = \begin{cases} 1, & \text{for } \bar{z} > 0; \\ 0, & \text{for } \bar{z} = 0; \\ -1, & \text{for } \bar{z} < 0, \end{cases} \quad (10)$$

where $\bar{z} = z - z'$. Arnoldus and Foley have carried out interesting studies of traveling and evanescent parts of \widehat{G}_{3D} and the optical near field [4,5].

The determination of $\widehat{G}_{fs}(\vec{k}_{\parallel}; z, z'; \omega)$ in Equation (6) involves evaluation of $\widehat{G}_{3D}(\vec{k}_{\parallel}; z, z'; \omega)$ at $z = 0$ and $z' = 0$: This introduces the divergent quantity $\delta(z - z') \mapsto \delta(0)$, which is an artifact of our confinement of the plasma layer to a sheet of zero thickness. As an analysis of the original integral equation (Equation (1)), taking account of a small but finite layer thickness d would involve an integration “smearing” the $z, z' \sim$ variables over the small range of layer thickness d . We estimate its effect on the result in terms of a representation of $\delta(z - z')$ as the limit of the sequence of “square pulse” functions given by

$$\delta(z - z') = \lim_{d \rightarrow 0} \left[\frac{\eta_+ \left(\frac{d}{2} - |z - z'| \right)}{d} \right], \text{ so } \delta(0) \approx \frac{1}{d}, \quad (11)$$

for $z = z' \mapsto 0$. This estimate is dimensionally correct and may be expected to properly represent the order of magnitude of the result for small d in removing the divergent $\delta(0)$ -quantity. Thus, we have

$$\widehat{G}_{3D}(\vec{k}_{\parallel}; 0, 0; \omega) = -\frac{1}{2ik_z} \left\{ \widehat{I} - \frac{1}{q^2 \omega} \left[\vec{k}_{\parallel} \vec{k}_{\parallel} + \widehat{e}_z \widehat{e}_z \left(k_z^2 - \frac{2ik_z}{d} \right) \right] \right\}. \quad (12)$$

As the solution of Equation (6) involves $\widehat{G}_{fs}(\vec{k}_{\parallel}; z, 0; \omega)$ and the 3D matrix inversion of $\left[\widehat{I} - \gamma \widehat{G}_{3D}(\vec{k}_{\parallel}; 0, 0; \omega) \right]$, it is worthwhile to point out that

$$\widehat{G}_{fs}(\vec{k}_{\parallel}; z, 0; \omega) = \widehat{G}_{3D}(\vec{k}_{\parallel}; z, 0; \omega) \left[\widehat{I} - \gamma \widehat{G}_{3D}(\vec{k}_{\parallel}; 0, 0; \omega) \right]^{-1}. \quad (13)$$

The inversion of $\left[\widehat{I} - \gamma \widehat{G}_{3D}(\vec{k}_{\parallel}; 0, 0; \omega) \right]$ is straightforward due to the block diagonality of $\widehat{G}_{3D}(\vec{k}_{\parallel}; 0, 0; \omega)$ (Equation (12)), and the resulting elements of $\widehat{G}_{fs}(\vec{k}_{\parallel}; z, 0; \omega)$ are exhibited explicitly in full detail in Reference [4].

3. Dyadic Electromagnetic Green's Function for a Perforated 2D Plasmonic Layer with a Nano-Hole Embedded in a 3D Bulk Host Medium

Integral Equation for the 2D Electromagnetic Dyadic Helmholtz Green's Function for a Perforated Plasmonic Layer \widehat{G}_{hole} and Solution

The conductivity of a 2D quantum plasmonic layer perforated by a nano-scale aperture of area A in the $(x - y)$ plane can be represented by subtracting from $\widehat{\sigma}_{fs}^{(2D)}$ the part of the full sheet conductivity associated with the hole, $\widehat{\sigma}_{hole}^{(2D)}$ (Figure 2), so the effective conductivity $\widehat{\sigma}^{(2D)}$ is given by

$$\widehat{\sigma}^{(2D)}(\vec{r}, \vec{r}'; \omega) = \widehat{\sigma}_{fs}^{(2D)}(\vec{r}, \vec{r}'; \omega) - \widehat{\sigma}_{hole}^{(2D)}(\vec{r}, \vec{r}'; \omega). \quad (14)$$

The corresponding dyadic electromagnetic Green's function for the perforated sheet, \widehat{G}_{hole} , obeys an integral equation relating it to \widehat{G}_{fs} as follows (position–frequency representation):

$$\begin{aligned} \widehat{G}_{hole}(\vec{r}, \vec{r}'; \omega) &= \widehat{G}_{fs}(\vec{r}, \vec{r}'; \omega) \\ &- \frac{4\pi i \omega}{c^2} \int d^3 \vec{r}'' \int d^3 \vec{r}''' \widehat{G}_{fs}(\vec{r}, \vec{r}''; \omega) \widehat{\sigma}_{hole}^{2D}(\vec{r}'', \vec{r}'''; \omega) \widehat{G}_{hole}(\vec{r}''', \vec{r}'; \omega). \end{aligned} \quad (15)$$

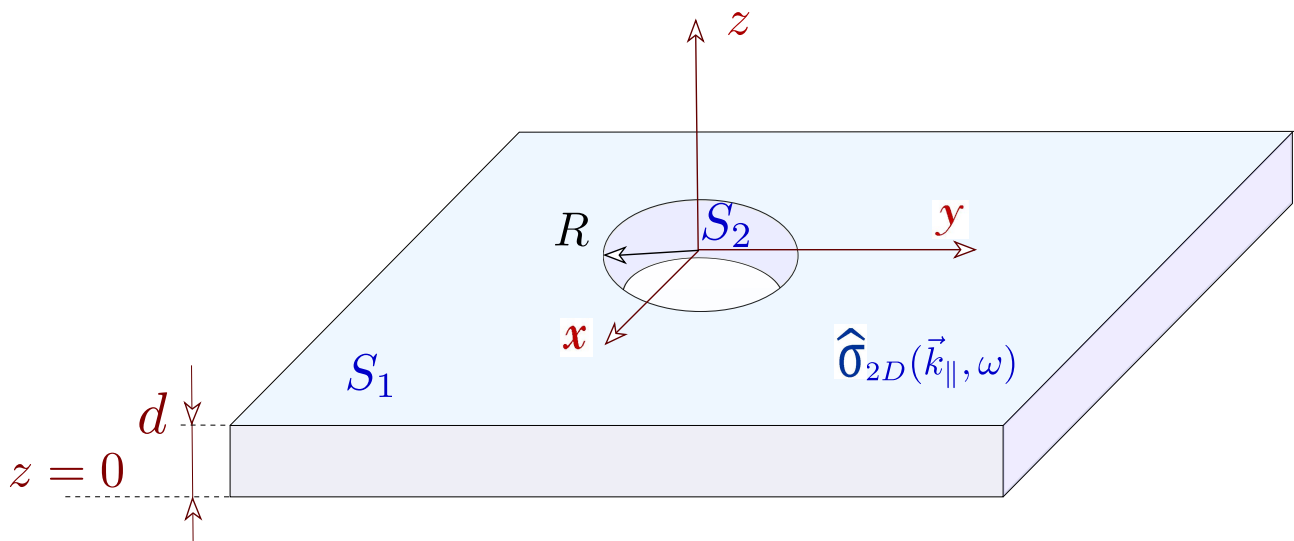


Figure 2. (Color online). Schematic representation of a perforated 2D plasmonic layer (thickness d , embedded at $z = 0$ in a three-dimensional bulk medium) with a nano-hole of radius R at the origin of the $(x - y)$ -plane.

The excised part of the conductivity defining the hole is described by the spatially localized conductivity tensor given by

$$\begin{aligned} \hat{\sigma}_{hole}^{(2D)}(x, x'; y, y'; z, z'; \omega) &= \hat{I}\sigma_{fs}^{(2D)}(\omega)\eta_+\left(\frac{a}{2} - |x|\right)\eta_+\left(\frac{a'}{2} - |x'|\right) \\ &\times \eta_+\left(\frac{b}{2} - |y|\right)\eta_+\left(\frac{b'}{2} - |y'|\right)\delta(z)\delta(z'), \end{aligned} \quad (16)$$

where $\sigma_{fs}^{(2D)}(\omega)$ is given by Equation (5) and $\eta_+(x)$ is the Heaviside unit step function confining the integration range on the 2D sheet to the subwavelength nano-hole dimensions (a, b) in the (x, y) directions. In considering small hole dimensions, $(a \mapsto 0; b \mapsto 0)$, we again note that the following limit of the sequence of “square pulse” functions

$$\lim_{a \rightarrow 0} \left[\frac{\eta_+\left(\frac{a}{2} - |x|\right)}{a} \right] = \delta(x) \quad (17)$$

is a representation of the “contact potential”-like Dirac delta function $\delta(x)$, whence we write

$$\hat{\sigma}_{hole}^{(2D)}(\vec{r}_{\parallel}, \vec{r}'_{\parallel}; z, z'; \omega) \approx \hat{I}A^2\sigma_{fs}^{(2D)}(\omega)\delta^{2D}(\vec{r}_{\parallel})\delta^{2D}(\vec{r}'_{\parallel})\delta(z)\delta(z'), \quad (18)$$

where $A = ab = a'b'$ is the area of the nano-hole. Employing Equation (18) in Equation (15), the integrations yield an algebraic solution for \hat{G}_{hole} in terms of \hat{G}_{fs} as

$$\hat{G}_{hole}(\vec{r}_{\parallel}, \vec{r}'_{\parallel}; z, z'; \omega) = \hat{G}_{fs}(\vec{r}_{\parallel}, \vec{r}'_{\parallel}; z, z'; \omega) - \beta \hat{G}_{fs}(\vec{r}_{\parallel}, 0; z, 0; \omega) \hat{G}_{hole}(0, \vec{r}'_{\parallel}; 0, z'; \omega), \quad (19)$$

where

$$\beta = \gamma A^2 = \left(\frac{4i\pi\omega}{c^2} \sigma_{fs}^{(2D)}(\omega) \right) A^2. \quad (20)$$

The algebraic solution of Equation (19) setting $\vec{r}_{\parallel} = 0$ and $z = 0$ yields

$$\hat{G}_{hole}(0, \vec{r}'_{\parallel}; 0, z'; \omega) = \left[\hat{I} + \beta \hat{G}_{fs}(0, 0; 0, 0; \omega) \right]^{-1} \hat{G}_{fs}(0, \vec{r}'_{\parallel}; 0, z'; \omega), \quad (21)$$

so we obtain an exact solution for the electromagnetic dyadic “hole” Green’s function as

$$\begin{aligned}\widehat{G}_{hole}(\vec{r}_{\parallel}, \vec{r}'_{\parallel}; z, z'; \omega) &= \widehat{G}_{fs}(\vec{r}_{\parallel}, \vec{r}'_{\parallel}; z, z'; \omega) \\ &- \beta \widehat{G}_{fs}(\vec{r}_{\parallel}, 0; z, 0; \omega) \left[\widehat{I} + \beta \widehat{G}_{fs}(0, 0; 0, 0; \omega) \right]^{-1} \widehat{G}_{fs}(0, \vec{r}'_{\parallel}; 0, z'; \omega).\end{aligned}\quad (22)$$

$\widehat{G}_{hole}(\vec{r}_{\parallel}, 0; z, 0; \omega)$ is of particular importance in assessing electromagnetic wave transmission/diffraction through the nano-hole, and it may be written as

$$\widehat{G}_{hole}(\vec{r}_{\parallel}, 0; z, 0; \omega) = \widehat{G}_{fs}(\vec{r}_{\parallel}, 0; z, 0; \omega) \left[\widehat{I} + \beta \widehat{G}_{fs}(0, 0; 0, 0; \omega) \right]^{-1}.\quad (23)$$

The denominator term $\widehat{G}_{fs}(0, 0; 0, 0; \omega)$ involves a divergent integral due to confinement of the nano-hole to a single point by its Dirac delta function representation. In recognition that the nano-hole actually has a small, finite radius R and that there is an associated “smearing” in the original integral equation, we note that in lateral wavenumber representation,

$$\widehat{G}_{fs}(0, 0; 0, 0; \omega) = \frac{1}{2\pi} \int_0^{\infty} dk_{\parallel} k_{\parallel} \widehat{G}_{fs}(\vec{k}_{\parallel}; 0, 0; \omega),\quad (24)$$

the divergence may be removed (“regularization”) by introducing a cut-off of the k_{\parallel} -integration range, namely that $k_{\parallel} < 1/R$ for nano-holes of subwavelength dimension R .

Finally, in lateral wavenumber representation, we find [1–3]

$$\widehat{G}_{hole}(\vec{r}_{\parallel}, 0; z, 0; \omega) = \begin{bmatrix} \frac{G_{fs}^{xx}(\vec{r}_{\parallel}, 0; z, 0; \omega)}{1 + \beta G_{fs}^{xx}(0, 0; 0, 0; \omega)} & 0 & \frac{G_{fs}^{yz}(\vec{r}_{\parallel}, 0; z, 0; \omega)}{1 + \beta G_{fs}^{zz}(0, 0; 0, 0; \omega)} \\ 0 & \frac{G_{fs}^{yy}(\vec{r}_{\parallel}, 0; z, 0; \omega)}{1 + \beta G_{fs}^{yy}(0, 0; 0, 0; \omega)} & 0 \\ \frac{G_{fs}^{zx}(\vec{r}_{\parallel}, 0; z, 0; \omega)}{1 + \beta G_{fs}^{xx}(0, 0; 0, 0; \omega)} & 0 & \frac{G_{fs}^{zz}(\vec{r}_{\parallel}, 0; z, 0; \omega)}{1 + \beta G_{fs}^{zz}(0, 0; 0, 0; \omega)} \end{bmatrix},\quad (25)$$

which represents the electromagnetic dyadic Green’s function \widehat{G}_{hole} of the perforated quantum plasmonic sheet system in the presence of the aperture, expressed explicitly in terms of \widehat{G}_{fs} elements. The requisite matrix inversions and integrations are carried out in detail in Ref. [2], and in the next section, we present a full graphical exposition of $\widehat{G}_{hole}(\vec{r}_{\parallel}, 0; z, 0; \omega)$ as a function of position, based on our numerical evaluation of the exact analytical solutions for the matrix elements of $\widehat{G}_{hole}(\vec{r}_{\parallel}, 0; z, 0; \omega)$ set forth in References [1–3].

4. Numerical Results

Our numerical evaluations of the real and imaginary parts of the five non-vanishing dyadic Green’s function matrix elements of Equation (25), $\text{Re}[\widehat{G}_{hole}(\vec{r}_{\parallel}, 0; z, 0; \omega)]$ and $\text{Im}[\widehat{G}_{hole}(\vec{r}_{\parallel}, 0; z, 0; \omega)]$, respectively, are presented in graphical form in both 3D and density plots below in Figures 3–17 as functions of x and y for frequency $f = 300$ THz. These numerical evaluations are exhibited for several values of distance z away from the layer screen: We chose $z = 50R$ (near-field), $z = 300R$ (middle-field) and $z = 1000R$ (far-field). These figures reveal the structure of the Green’s function elements for the perforated layer in terms of near-field ($z = 50R$), middle-field ($z = 300R$) and far-field ($z = 1000R$) zones for $R = 5$ nm. Our use of the terms “near-field”, “middle-field” and “far-field” do *not* have the usual reference to distance from a center at the nano-hole relative to wavelength; instead, these terms are used here for describing z - distance from the plasmonic layer relative to wavelength $\lambda = \frac{2\pi}{q\omega}$. (This includes, for example, that a “near-field” figure exhibits results at both large and small lateral \vec{r}_{\parallel} -distances from the nano-hole so long as the z -distance is small in relation to wavelength, etc.). In summary, near-field is defined as $\frac{z}{\lambda} \ll 1$, middle-field as $\frac{z}{\lambda} \sim 1$ and far-field as $\frac{z}{\lambda} \gg 1$.

NOTATION: IN ALL FIGURES BELOW $\widehat{G}_{hole} \equiv \widehat{G}$.

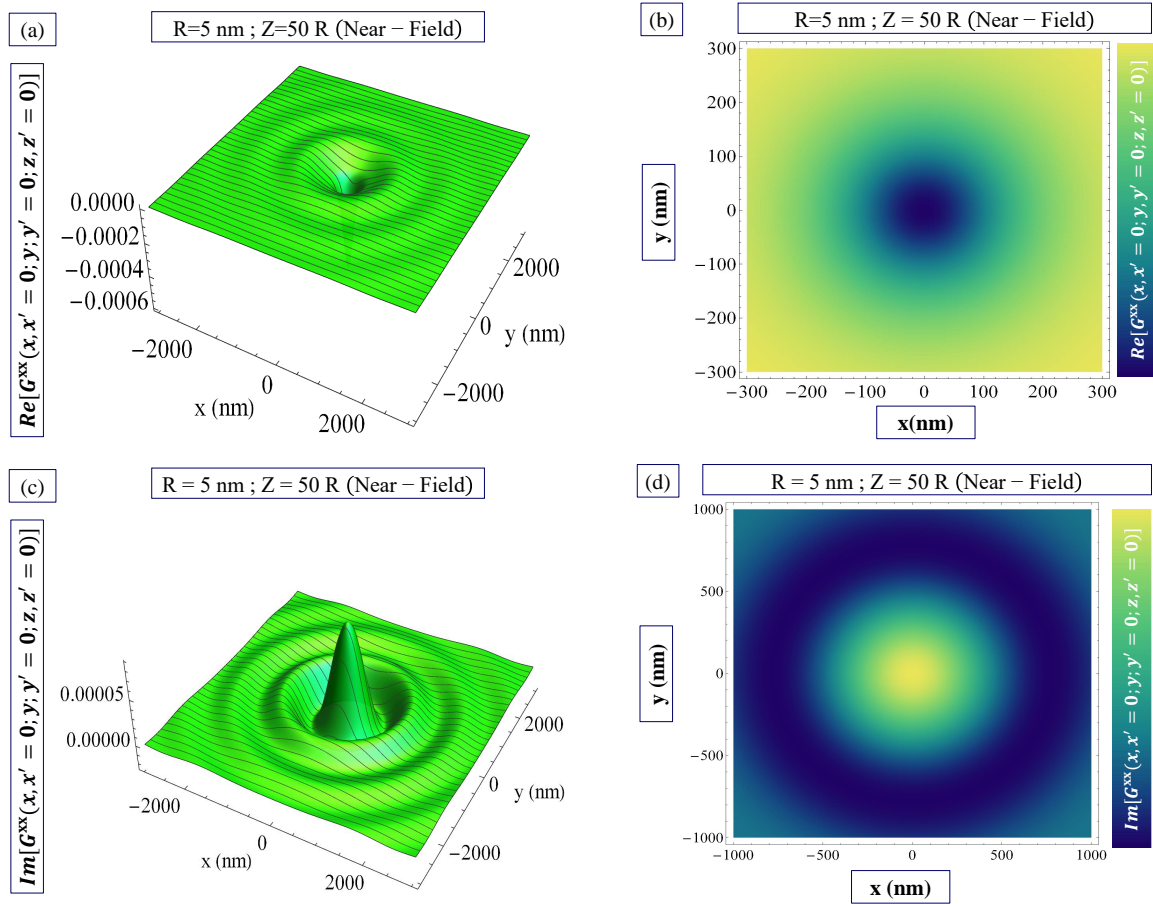


Figure 3. (Color online). Figures (a,b) exhibit $\text{Re}[G^{xx}(\vec{r}_{\parallel}, 0; z, 0; \omega)]$ and (c,d) present $\text{Im}[G^{xx}(\vec{r}_{\parallel}, 0; z, 0; \omega)]$ (in 3D (a,c) and density (b,d) plots) for a perforated 2D plasmonic layer of GaAs in the presence of a nano-hole of radius $R = 5 \text{ nm}$ at $z = 50R$ (Near-Field) for $\epsilon_b = 1$, $n_{2D} = 4 \times 10^{15} \text{ cm}^{-2}$, $d = 10 \text{ nm}$ and $m^* = 0.065m_0$ where m_0 is the free-electron mass.

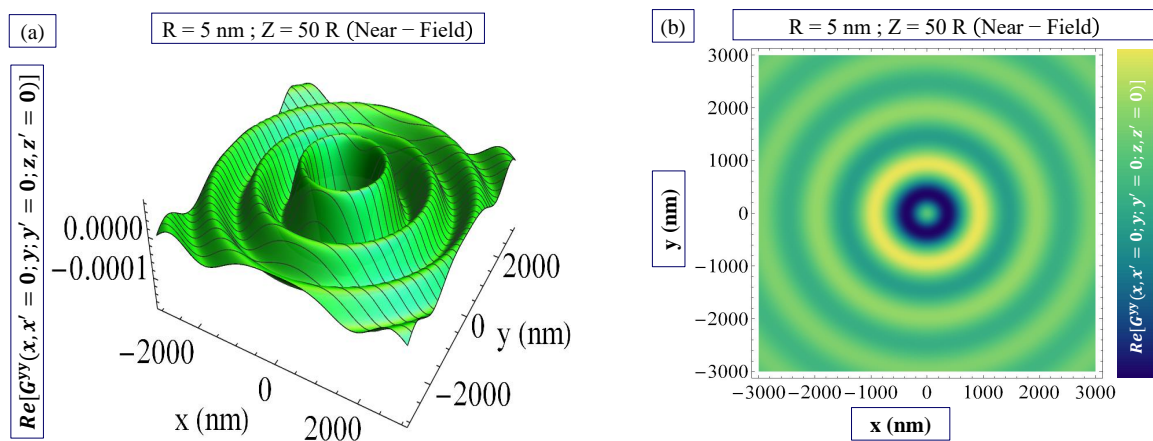


Figure 4. Cont.

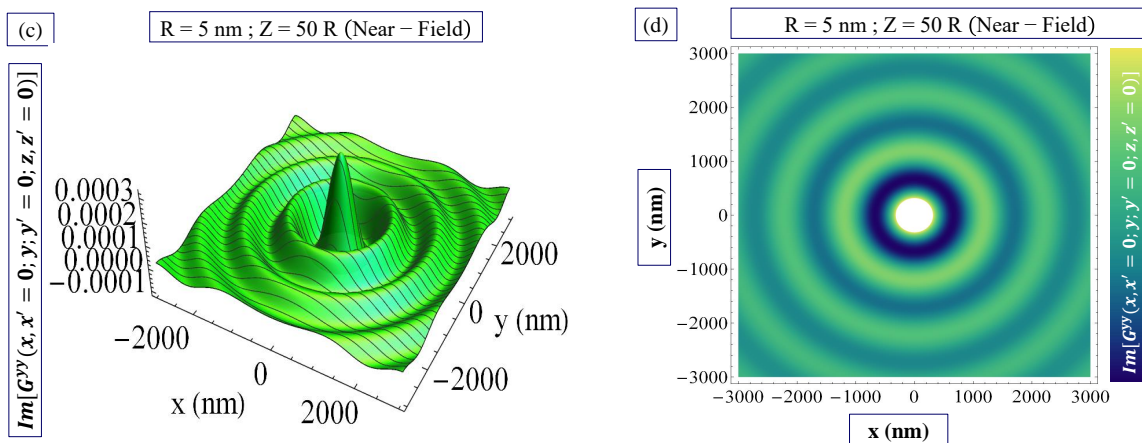


Figure 4. (Color online). Figures (a,b) exhibit $\text{Re}[G^{yy}(\vec{r}_{\parallel}, 0; z, 0; \omega)]$ and (c,d) present $\text{Im}[G^{yy}(\vec{r}_{\parallel}, 0; z, 0; \omega)]$ (in 3D (a,c) and density (b,d) plots) for a perforated 2D plasmonic layer of GaAs in the presence of a nano-hole of radius $R = 5 \text{ nm}$ at $z = 50 R$ (Near-Field) for $\epsilon_b = 1$, $n_{2D} = 4 \times 10^{15} \text{ cm}^{-2}$, $d = 10 \text{ nm}$ and $m^* = 0.065m_0$ where m_0 is the free-electron mass.

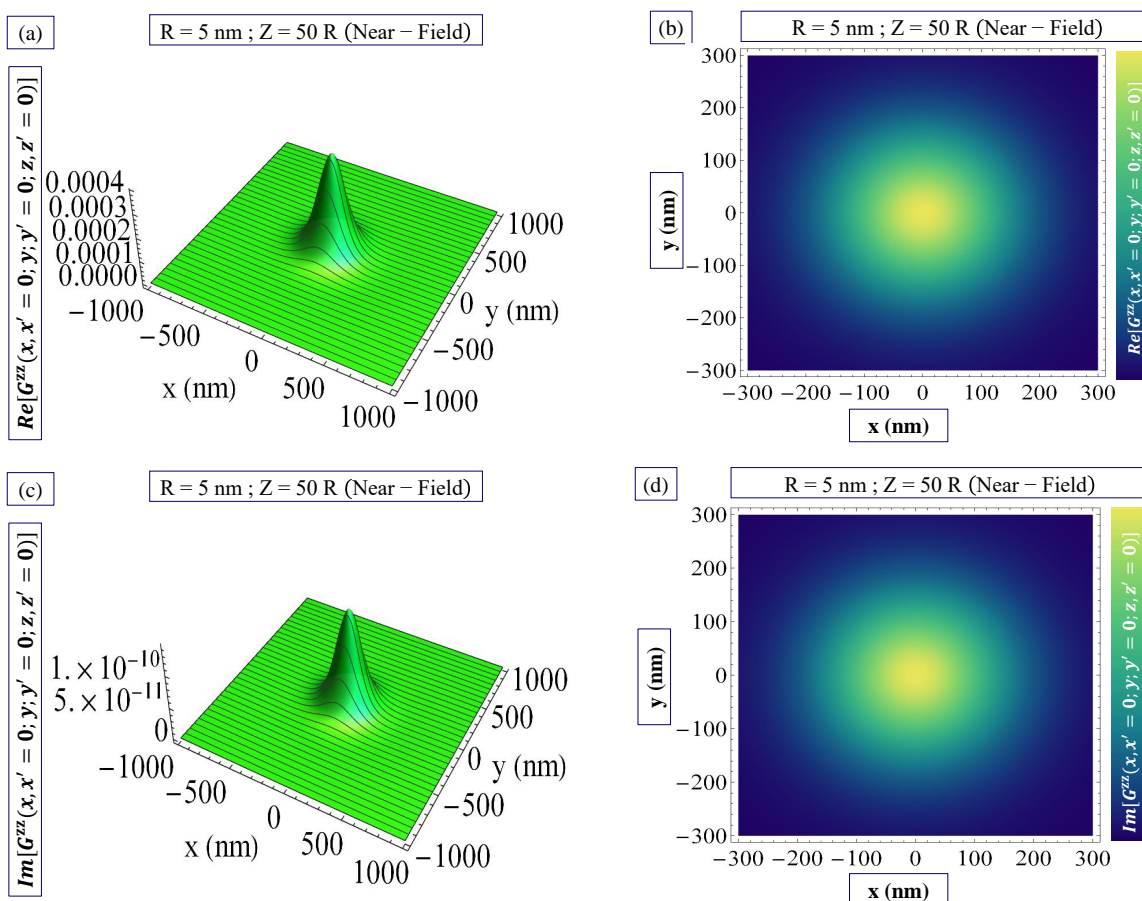


Figure 5. (Color online). Figures (a,b) exhibit $\text{Re}[G^{zz}(\vec{r}_{\parallel}, 0; z, 0; \omega)]$ and (c,d) present $\text{Im}[G^{zz}(\vec{r}_{\parallel}, 0; z, 0; \omega)]$ (in 3D (a,c) and density (b,d) plots) for a perforated 2D plasmonic layer of GaAs in the presence of a nano-hole of radius $R = 5 \text{ nm}$ at $z = 50 R$ (Near-Field) for $\epsilon_b = 1$, $n_{2D} = 4 \times 10^{15} \text{ cm}^{-2}$, $d = 10 \text{ nm}$ and $m^* = 0.065m_0$ where m_0 is the free-electron mass.

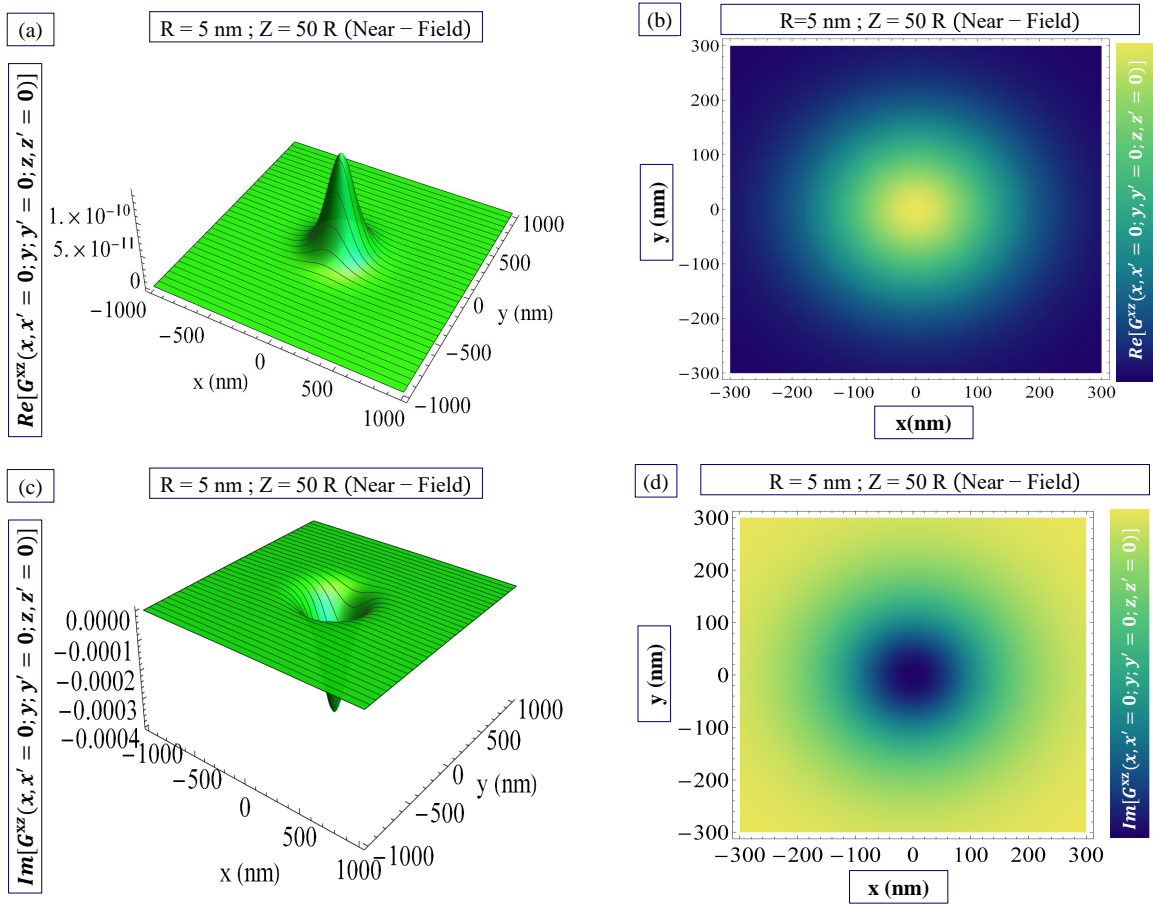


Figure 6. (Color online). Figures (a,b) exhibit $\text{Re}[G^{xz}(\vec{r}_{\parallel}, 0; z, 0; \omega)]$ and (c,d) present $\text{Im}[G^{xz}(\vec{r}_{\parallel}, 0; z, 0; \omega)]$ (in 3D (a,c) and density (b,d) plots) for a perforated 2D plasmonic layer of GaAs in the presence of a nano-hole of radius $R = 5 \text{ nm}$ at $z = 50 R$ (Near-Field) for $\epsilon_b = 1$, $n_{2D} = 4 \times 10^{15} \text{ cm}^{-2}$, $d = 10 \text{ nm}$ and $m^* = 0.065m_0$ where m_0 is the free-electron mass.

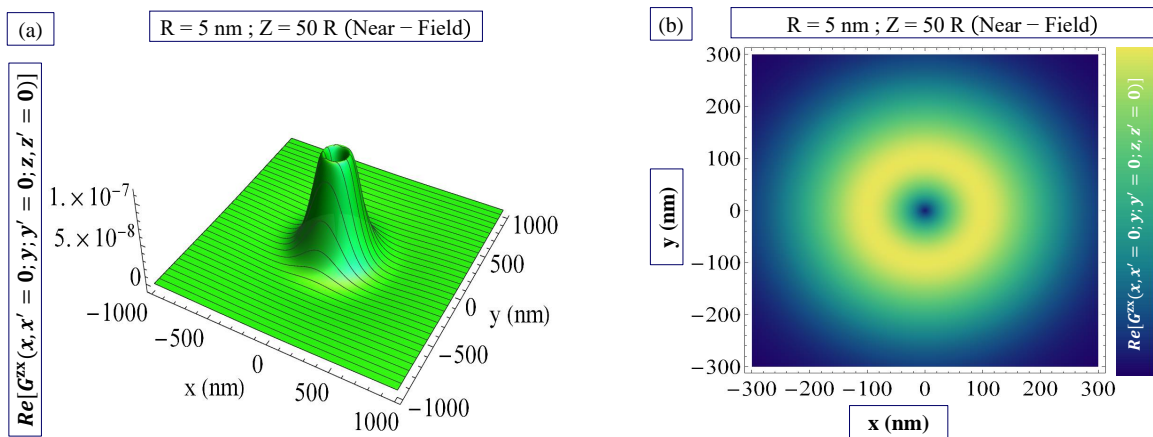


Figure 7. Cont.

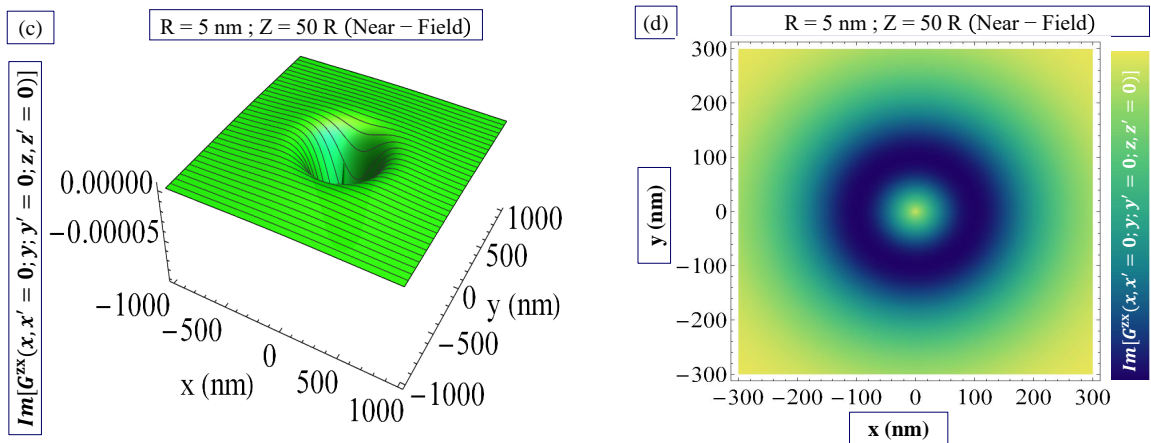


Figure 7. (Color online). Figures (a,b) exhibit $\text{Re}[G^{zx}(\vec{r}_{\parallel}, 0; z, 0; \omega)]$ and (c,d) present $\text{Im}[G^{zx}(\vec{r}_{\parallel}, 0; z, 0; \omega)]$ (in 3D (a,c) and density (b,d) plots) for a perforated 2D plasmonic layer of GaAs in the presence of a nano-hole of radius $R = 5 \text{ nm}$ at $z = 50 R$ (Near-Field) for $\epsilon_b = 1$, $n_{2D} = 4 \times 10^{15} \text{ cm}^{-2}$, $d = 10 \text{ nm}$ and $m^* = 0.065m_0$ where m_0 is the free-electron mass.

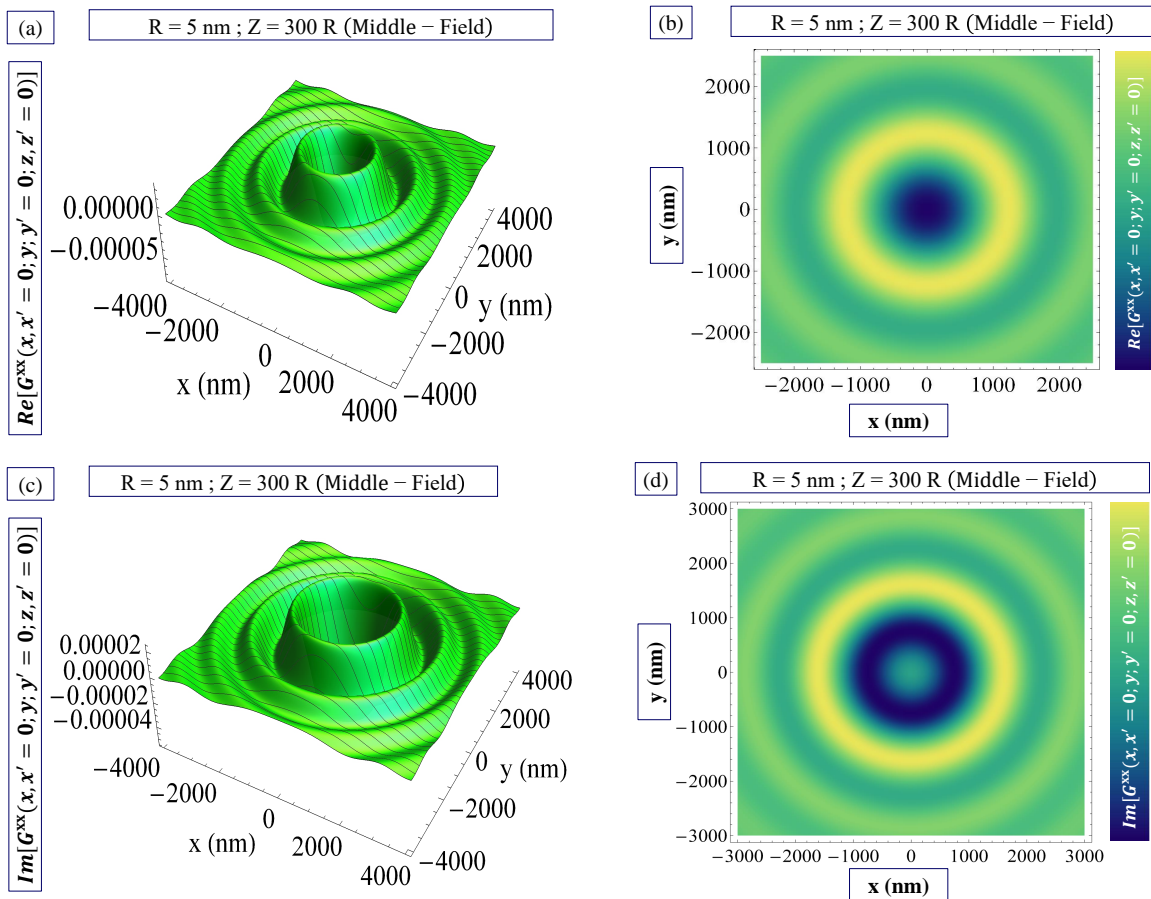


Figure 8. (Color online). Figures (a,b) exhibit $\text{Re}[G^{xx}(\vec{r}_{\parallel}, 0; z, 0; \omega)]$ and (c,d) present $\text{Im}[G^{xx}(\vec{r}_{\parallel}, 0; z, 0; \omega)]$ (in 3D (a,c) and density (b,d) plots) for a perforated 2D plasmonic layer of GaAs in the presence of a nano-hole of radius $R = 5 \text{ nm}$ at $z = 300 R$ (Middle-Field) for $\epsilon_b = 1$, $n_{2D} = 4 \times 10^{15} \text{ cm}^{-2}$, $d = 10 \text{ nm}$ and $m^* = 0.065m_0$ where m_0 is the free-electron mass.

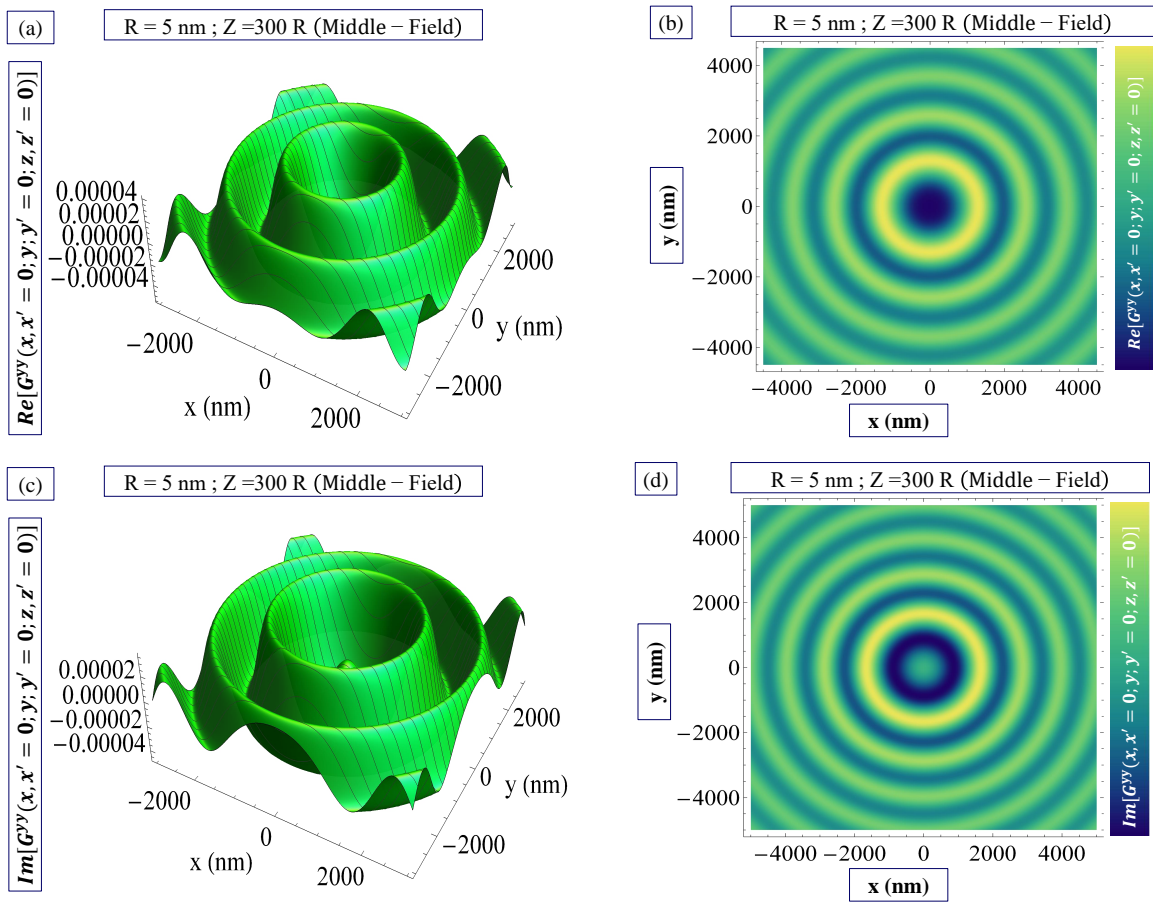


Figure 9. (Color online). Figures (a,b) exhibit $\text{Re}[G^{yy}(\vec{r}_{\parallel}, 0; z, 0; \omega)]$ and (c,d) present $\text{Im}[G^{yy}(\vec{r}_{\parallel}, 0; z, 0; \omega)]$ (in 3D (a,c) and density (b,d) plots) for a perforated 2D plasmonic layer of GaAs in the presence of a nano-hole of radius $R = 5 \text{ nm}$ at $z = 300 R$ (Middle-Field) for $\epsilon_b = 1$, $n_{2D} = 4 \times 10^{15} \text{ cm}^{-2}$, $d = 10 \text{ nm}$ and $m^* = 0.065m_0$ where m_0 is the free-electron mass.

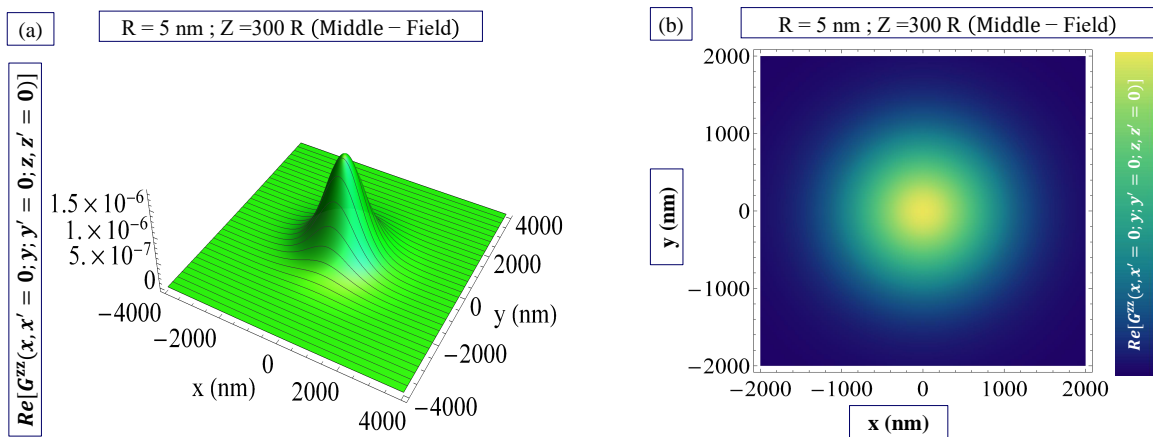


Figure 10. Cont.

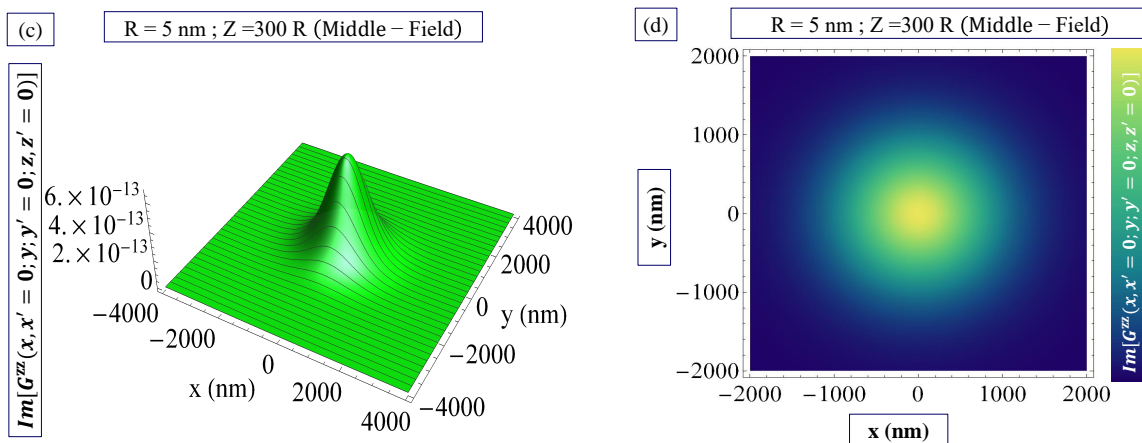


Figure 10. (Color online). Figures (a,b) exhibit $\text{Re}[G^{zz}(\vec{r}_{\parallel}, 0; z, 0; \omega)]$ and (c,d) present $\text{Im}[G^{zz}(\vec{r}_{\parallel}, 0; z, 0; \omega)]$ (in 3D (a,c) and density (b,d) plots) for a perforated 2D plasmonic layer of GaAs in the presence of a nano-hole of radius $R = 5 \text{ nm}$ at $z = 300 R$ (Middle-Field) for $\epsilon_b = 1$, $n_{2D} = 4 \times 10^{15} \text{ cm}^{-2}$, $d = 10 \text{ nm}$ and $m^* = 0.065m_0$ where m_0 is the free-electron mass.

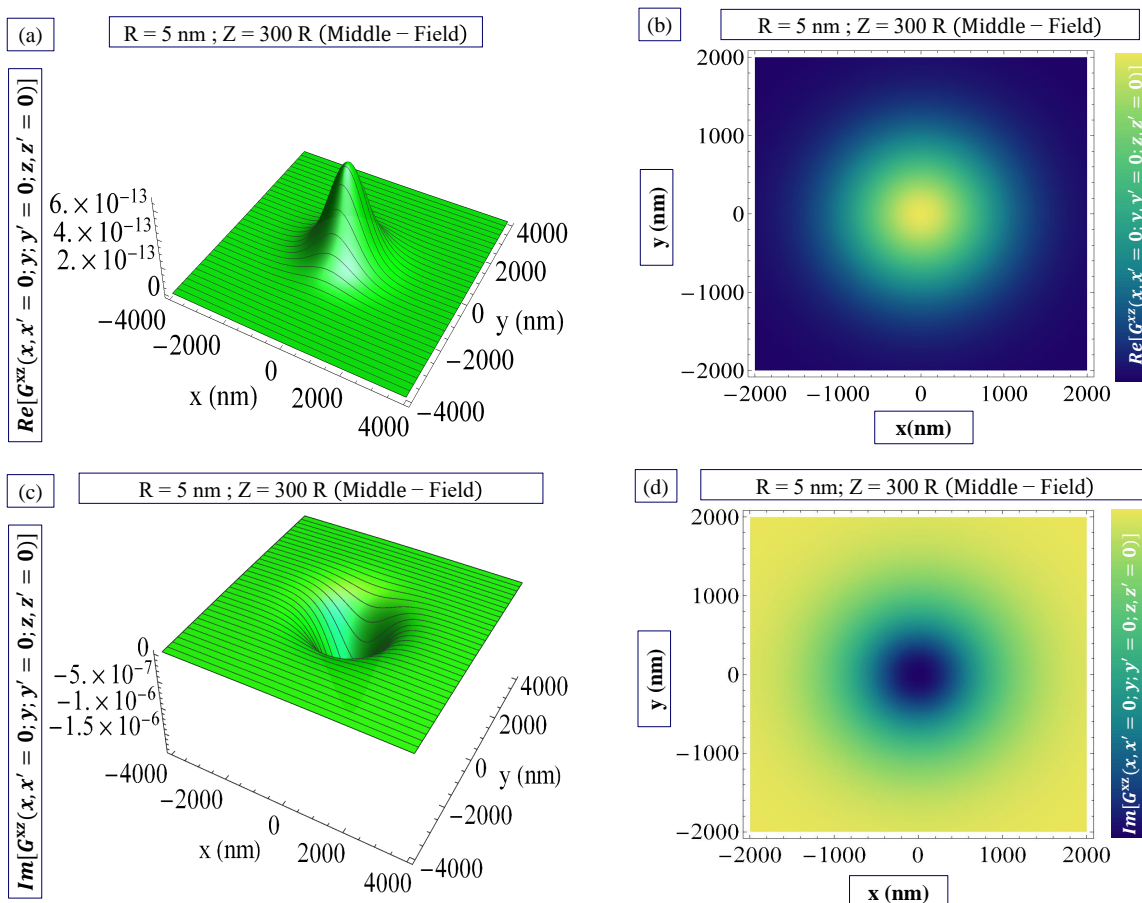


Figure 11. (Color online). Figures (a,b) exhibit $\text{Re}[G^{xz}(\vec{r}_{\parallel}, 0; z, 0; \omega)]$ and (c,d) present $\text{Im}[G^{xz}(\vec{r}_{\parallel}, 0; z, 0; \omega)]$ (in 3D (a,c) and density (b,d) plots) for a perforated 2D plasmonic layer of GaAs in the presence of a nano-hole of radius $R = 5 \text{ nm}$ at $z = 300 R$ (Middle-Field) for $\epsilon_b = 1$, $n_{2D} = 4 \times 10^{15} \text{ cm}^{-2}$, $d = 10 \text{ nm}$ and $m^* = 0.065m_0$ where m_0 is the free-electron mass.

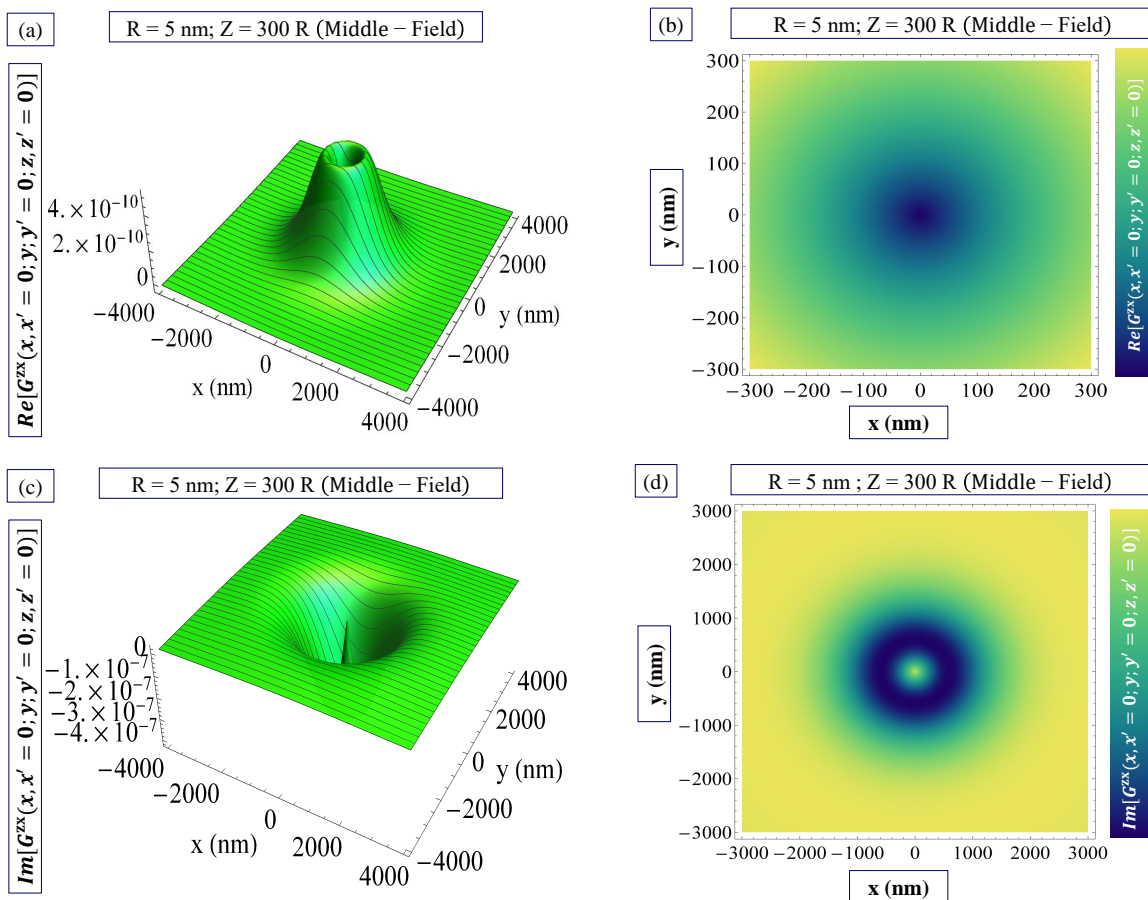


Figure 12. (Color online). Figures (a,b) exhibit $\text{Re}[G^{zx}(\vec{r}_{\parallel}, 0; z, 0; \omega)]$ and (c,d) present $\text{Im}[G^{zx}(\vec{r}_{\parallel}, 0; z, 0; \omega)]$ (in 3D (a,c) and density (b,d) plots) for a perforated 2D plasmonic layer of GaAs in the presence of a nano-hole of radius $R = 5 \text{ nm}$ at $z = 1000 R$ (Far-Field) for $\epsilon_b = 1$, $n_{2D} = 4 \times 10^{15} \text{ cm}^{-2}$, $d = 10 \text{ nm}$ and $m^* = 0.065m_0$ where m_0 is the free-electron mass.

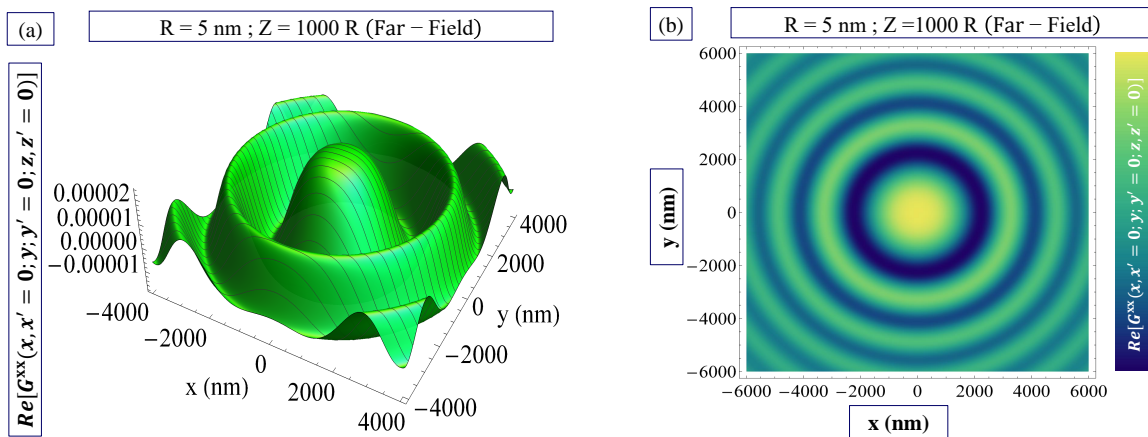


Figure 13. Cont.

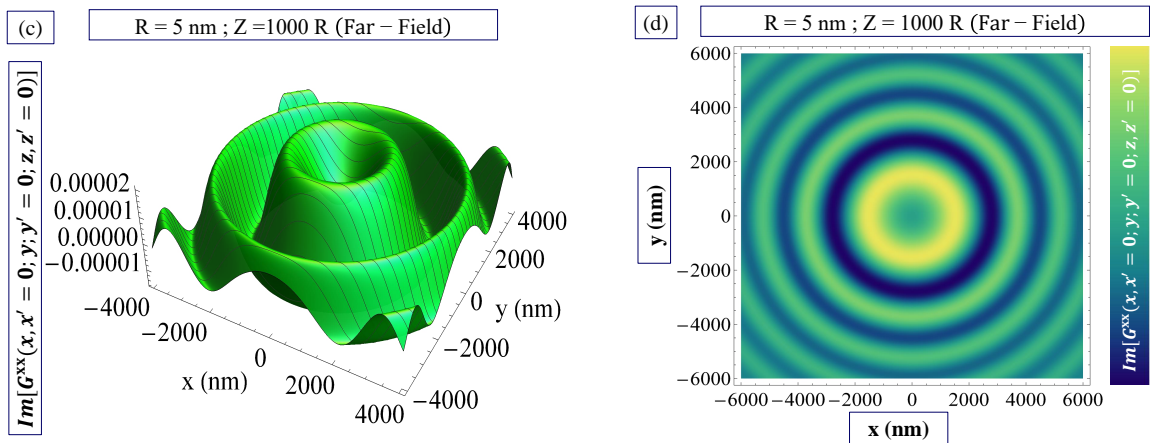


Figure 13. (Color online). Figures (a,b) exhibit $\text{Re}[G^{xx}(\vec{r}_{\parallel}, 0; z, 0; \omega)]$ and (c,d) present $\text{Im}[G^{xx}(\vec{r}_{\parallel}, 0; z, 0; \omega)]$ (in 3D (a,c) and density (b,d) plots) for a perforated 2D plasmonic layer of GaAs in the presence of a nano-hole of radius $R = 5$ nm at $z = 1000 R$ (Far-Field) for $\epsilon_b = 1$, $n_{2D} = 4 \times 10^{15} \text{ cm}^{-2}$, $d = 10$ nm and $m^* = 0.065m_0$ where m_0 is the free-electron mass.

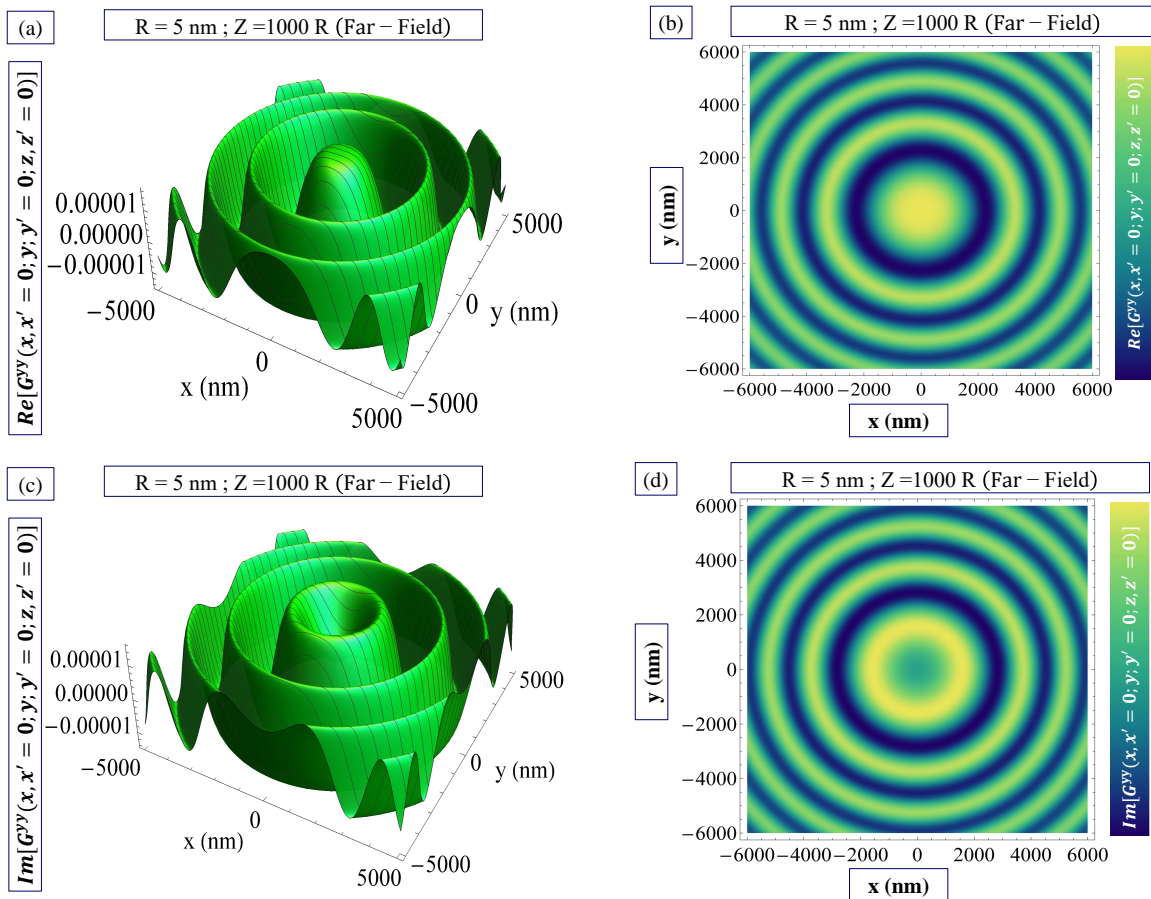


Figure 14. (Color online). Figures (a,b) exhibit $\text{Re}[G^{yy}(\vec{r}_{\parallel}, 0; z, 0; \omega)]$ and (c,d) present $\text{Im}[G^{yy}(\vec{r}_{\parallel}, 0; z, 0; \omega)]$ (in 3D (a,c) and density (b,d) plots) for a perforated 2D plasmonic layer of GaAs in the presence of a nano-hole of radius $R = 5$ nm at $z = 1000 R$ (Far-Field) for $\epsilon_b = 1$, $n_{2D} = 4 \times 10^{15} \text{ cm}^{-2}$, $d = 10$ nm and $m^* = 0.065m_0$ where m_0 is the free-electron mass.

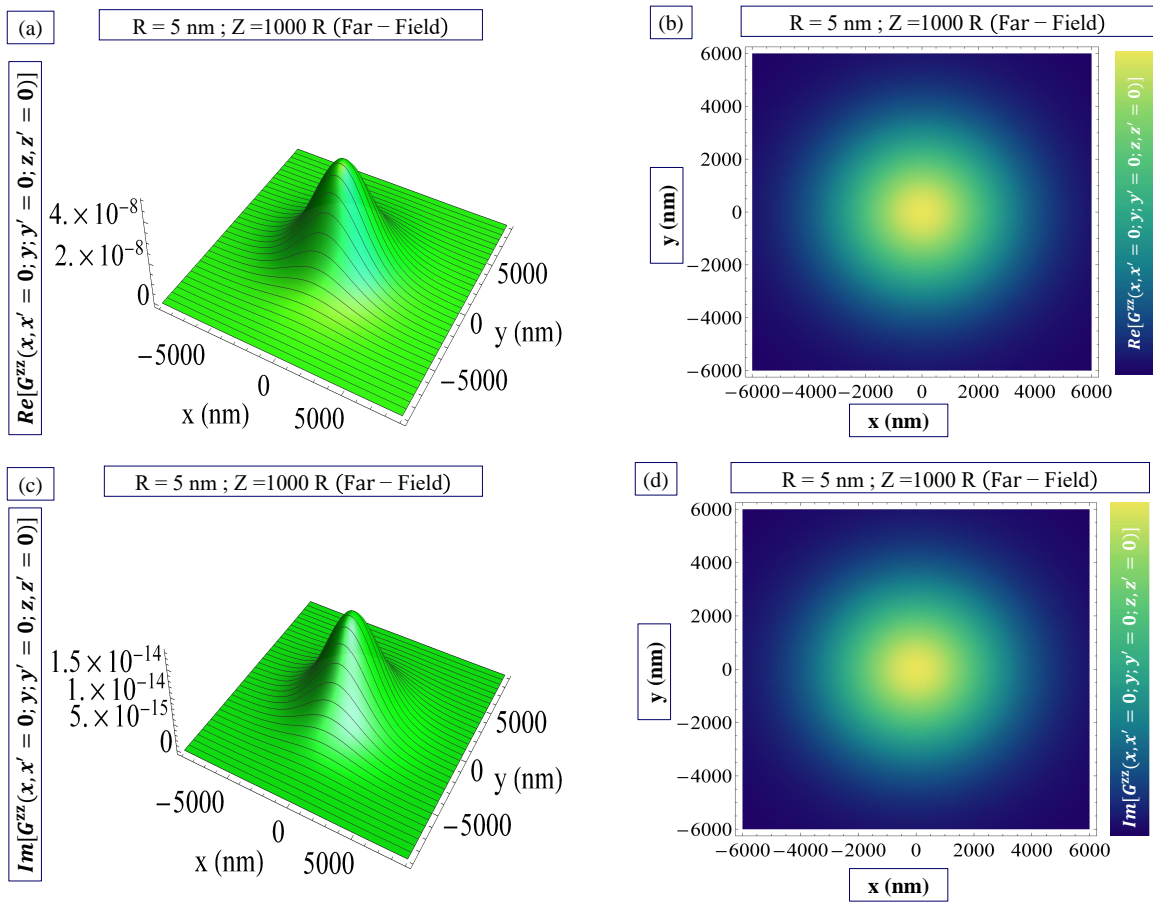


Figure 15. (Color online). Figures (a,b) exhibit $\text{Re}[G^{zz}(\vec{r}_{\parallel}, 0; z, 0; \omega)]$ and (c,d) present $\text{Im}[G^{zz}(\vec{r}_{\parallel}, 0; z, 0; \omega)]$ (in 3D (a,c) and density (b,d) plots) for a perforated 2D plasmonic layer of GaAs in the presence of a nano-hole of radius $R = 5 \text{ nm}$ at $z = 1000 R$ (Far-Field) for $\epsilon_b = 1$, $n_{2D} = 4 \times 10^{15} \text{ cm}^{-2}$, $d = 10 \text{ nm}$ and $m^* = 0.065m_0$ where m_0 is the free-electron mass.

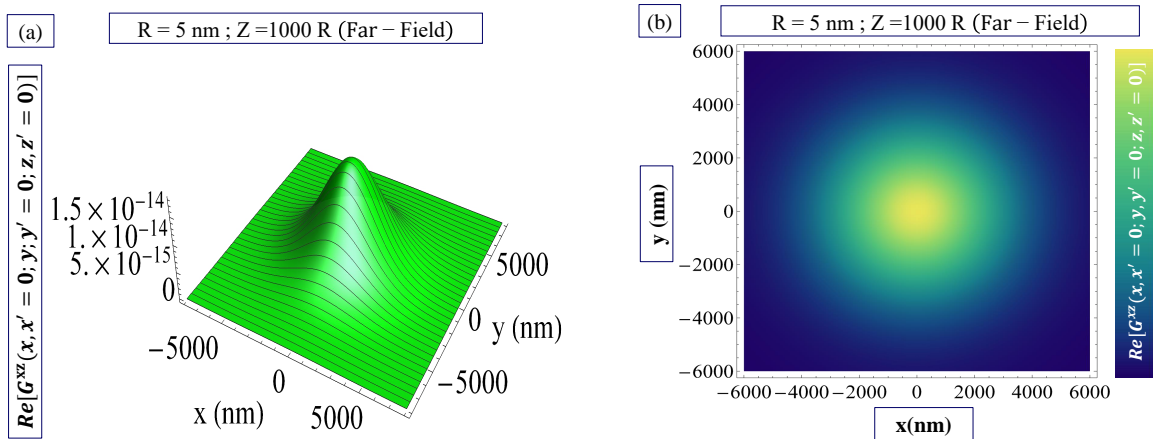


Figure 16. Cont.

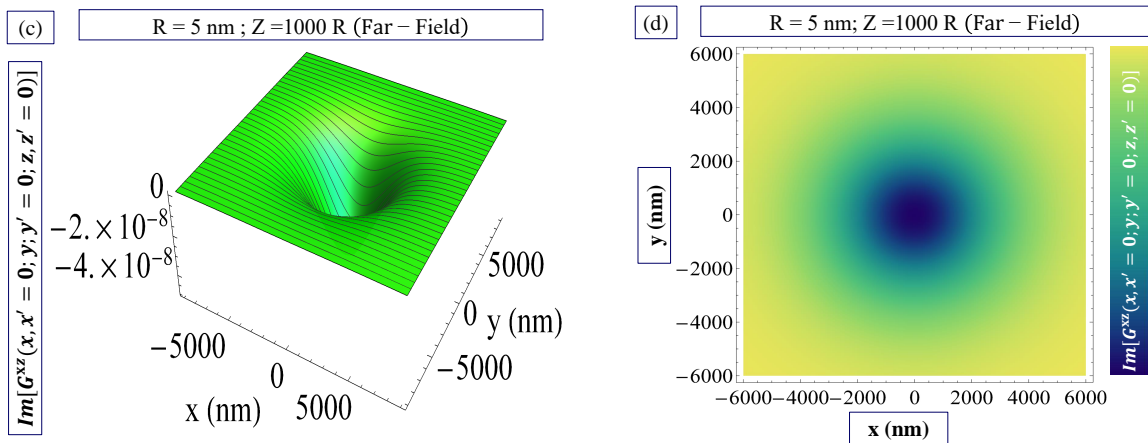


Figure 16. (Color online). Figures (a,b) exhibit $\text{Re}[G^{xz}(\vec{r}_{\parallel}, 0; z, 0; \omega)]$ and (c,d) present $\text{Im}[G^{xz}(\vec{r}_{\parallel}, 0; z, 0; \omega)]$ (in 3D (a,c) and density (b,d) plots) for a perforated 2D plasmonic layer of GaAs in the presence of a nano-hole of radius $R = 5 \text{ nm}$ at $z = 1000 R$ (Far-Field) for $\epsilon_b = 1$, $n_{2D} = 4 \times 10^{15} \text{ cm}^{-2}$, $d = 10 \text{ nm}$ and $m^* = 0.065m_0$ where m_0 is the free-electron mass.

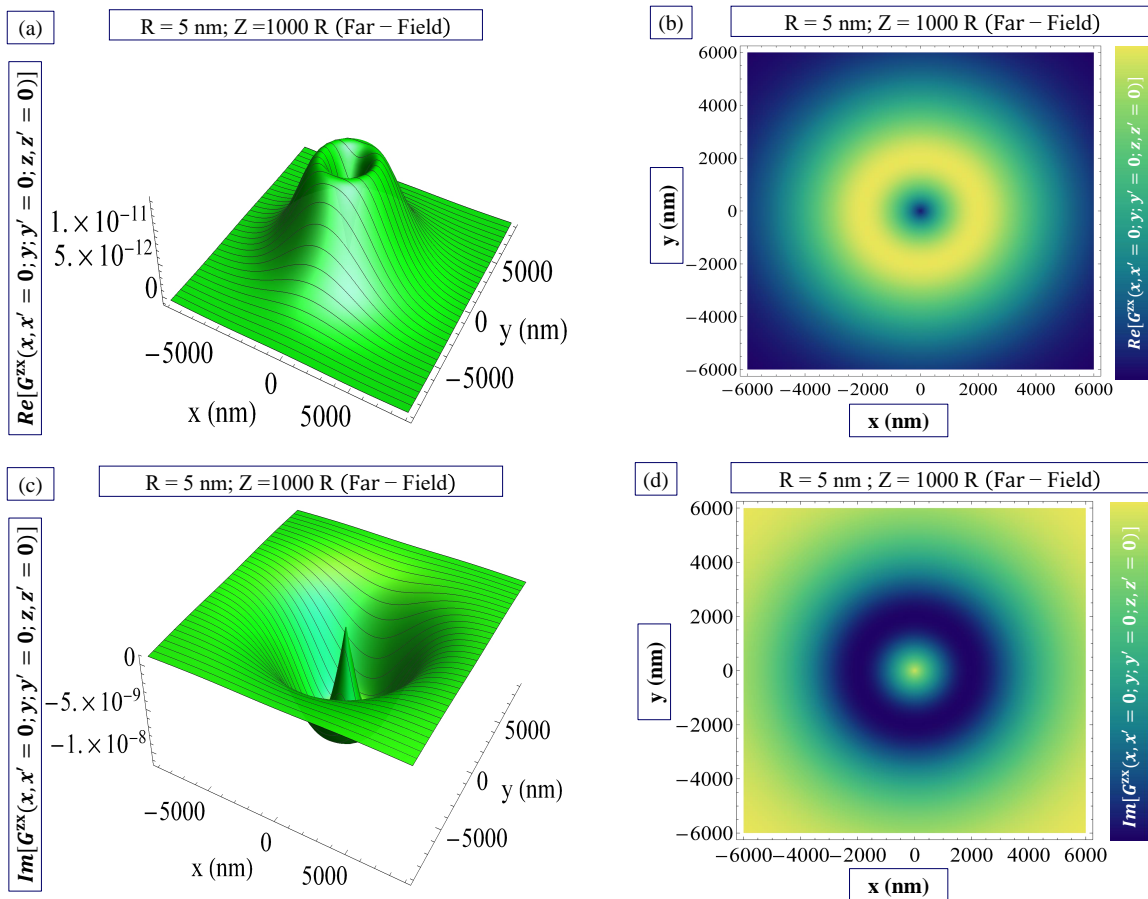


Figure 17. (Color online). Figures (a,b) exhibit $\text{Re}[G^{zx}(\vec{r}_{\parallel}, 0; z, 0; \omega)]$ and (c,d) present $\text{Im}[G^{zx}(\vec{r}_{\parallel}, 0; z, 0; \omega)]$ (in 3D (a,c) and density (b,d) plots) for a perforated 2D plasmonic layer of GaAs in the presence of a nano-hole of radius $R = 5 \text{ nm}$ at $z = 1000 R$ (Far-Field) for $\epsilon_b = 1$, $n_{2D} = 4 \times 10^{15} \text{ cm}^{-2}$, $d = 10 \text{ nm}$ and $m^* = 0.065m_0$ where m_0 is the free-electron mass.

5. Concluding Remarks

In this paper, we have discussed the exact analytic solution and its thorough numerical analysis for the closed-form expression of the dyadic electromagnetic Green's function of

a perforated, thin 2D quantum plasmonic layer embedded in a 3D host medium in the presence of a subwavelength nano-hole. This solution is exact and devoid of assumptions, having represented the perforation in terms of a “contact interaction”-like 2D Dirac delta function and having represented the 2D layer localization to the plane $z = 0$ in terms of a 1D Dirac delta function. Such exactness is elusive in earlier work and in classic approaches to the analysis of electromagnetic transmission problems involving diffraction. Our results for the Green’s function have been applied to a number of calculations of electromagnetic wave transmission/diffraction through a perforated plasmonic layer with a subwavelength nano-hole for both normal and non-normal incidence, including both nano-hole transmission/diffraction effects jointly with transmission through the entire plasma layer [1–3].

Earlier reports by Bethe [6] and Levine and Schwinger [7–9] have relied on the assumption that the screen is perfectly conducting and is represented by the associated metallic boundary conditions, which are simulated by the use of fictitious magnetic charges and currents. These reports also review the limitations of the classic diffraction studies of Kirchhoff, Stratton and Chu and Lord Rayleigh. Other important analyses of *resonant enhanced* and collimated EM wave transmission/diffraction by subwavelength slits in thick metal films have been reported by Kukhlevsky, Mechler, Csapo, Janssens and Samek [10,11] and Neerhoff and Mur [12]. This strong enhancement of light by subwavelength apertures is nicely reviewed by Genet and Ebbesen [13], who emphasize the important role of the interaction of the EM wave with electronic resonances in the surface of the metal film. Of course, the incident EM wavefield drives such electronic modes to subsequently re-radiate EM field contributions that add to the incident field to ensure the satisfaction of the perfect metal boundary conditions. It is in the context of these references that the present results are meaningful, albeit with significant contrast: Firstly, the limitation to perfect metal boundary conditions is *not* appropriate and is *not* employed here, as a layer of plasma has been addressed in our work, with *no* explicit reference to boundary conditions (which are implicit in the layer conductivity distribution). Secondly, we address a *thin* (2D) layer of plasma rather than a thick slab, and in our case, the interaction of the incident EM wave with the electronic resonances of the material is *explicitly* evident in the structure of the “hole” Green’s function of Equation (25), whose elements involve $[1 + \beta G_{fs}(0,0;0,0;\omega)]^{-1}$, and the corresponding dispersion relation, $\det[1 + \beta G_{fs}(0,0;0,0;\omega)] = 0$, identifies the 2D sheet polariton/plasmon resonant modes of the material system explicitly. Obviously, with this determinant in the denominator of the “hole” Green’s function, a driving frequency ω_{res} that causes the determinant to vanish leads to the resonant enhancement of the EM radiation by the excitation of the radiating 2D sheet polaritons/plasmons, which contribute to the transmitted electromagnetic field throughout the thin layer as well as through the aperture. Finally, we again emphasize that our results are *exact* within the framework of the “contact interaction”-like Dirac delta function representation of the material dimensions involved, which are pertinent to 2D/nano systems, and are not limited by other approximations like perfect metal boundary conditions.

The inspection of the resulting Green’s function elements exhibited in both 3D and density plots (above) shows that, for large $r_{\parallel} \mapsto x > 2500$ nm, the spatial dependence of the Green’s function for electromagnetic transmission/diffraction through the perforated plasmonic layer becomes oscillatory as a function of $r_{\parallel}(x)$ with peaks uniformly spaced. In this regard, it should be noted that our designation of near, middle and far zones is defined in terms of z -values (50R, 300R, 1000R) *alone*, to the exclusion of r_{\parallel} : In consequence of this exclusion, the figures actually carry useful information for r_{\parallel} in *all* radiation zones as conventionally defined in terms of the incident wavelength $\lambda \approx 2\pi/q\omega$. Furthermore, this approach to oscillatory behavior as a function of r_{\parallel} with uniformly spaced peaks is accompanied by a geometric $1/r_{\parallel}$ -diminution of the amplitude of the Green’s function. On the other hand, our far-zone figures also show that when $z < r_{\parallel} = x$, the Green’s function flattens as a function of $r_{\parallel} = x$ into a region of constancy. In connection with this, it should be borne in mind that the electromagnetic wave transmission occurs through the entire

thin plasmonic layer, as well as through the nano-hole aperture in the layer. For sufficiently large $r_{\parallel} > z$, the nano-hole contribution to transmission is relatively ineffective.

Author Contributions: D.M. carried out all numerical calculations. N.J.M.H. formulated and solved the coupled successive Green's function integral equations governing the system. H.L. verified the correctness of all numerical and analytical works in this paper. All authors have read and agreed to the published version of the manuscript.

Funding: This research was partially funded by the NSF-AGEP program.

Institutional Review Board Statement: Not applicable.

Informed Consent Statement: Not applicable.

Data Availability Statement: Not applicable.

Acknowledgments: We gratefully acknowledge support from the NSF-AGEP program for the work reported in this paper. Thanks are extended to M. L. Glasser and Erik Lenzing for numerous helpful discussions as well as Liuba Zhemchuzhna and Andrii Iurov for helpful comments.

Conflicts of Interest: The authors declare no conflict of interest.

References

1. Horing, N.J.M.; Bagaeva, T.Y.; Popov, V.V. Excitation of Radiative Polaritons in a Two-Dimensional Excitonic Layer by a Light Pulse. *J. Opt. Soc. Am. B* **2007**, *24*, 2428. [[CrossRef](#)]
2. Horing, N.J.M.; Miessein, D.; Gumbs, G. Electromagnetic Wave Transmission Through a Subwavelength Nano-hole in a Two-Dimensional Plasmonic Layer. *J. Opt. Soc. Am. A* **2015**, *32*, 1184–1198. [[CrossRef](#)] [[PubMed](#)]
3. Miessein, D.; Horing, N.J.M.; Lenzing, H.; Gumbs, G. Incident-Angle Dependence of Electromagnetic Transmission through a Plasmonic Screen with a Nano-Aperture. *Adv. Nano Bio. MD* **2017**, *1*, 54–70.
4. Arnoldus, H.F.; Foley, J.T. Traveling and evanescent parts of the electromagnetic Green's tensor. *J. Opt. Soc. Am. A* **2002**, *19*, 1701–1711. [[CrossRef](#)] [[PubMed](#)]
5. Arnoldus, H.F.; Foley, J.T. Travelling and evanescent parts of the optical near field. *J. Mod. Opt.* **2003**, *50*, 1883–1901. [[CrossRef](#)]
6. Bethe, H.A. Theory of Diffraction by Small Holes. *Phys. Rev.* **1944**, *66*, 163. [[CrossRef](#)]
7. Levine, H.; Schwinger, J. On the Theory of Electromagnetic Wave Diffraction by an Aperture in an Infinite Plane Conducting Screen. *Commun. Pure Appl. Math.* **1950**, *3*, 355–391. [[CrossRef](#)]
8. Levine, H.; Schwinger, J. On the Theory of Diffraction by an Aperture in an Infinite Plane Screen. I. *Phys. Rev.* **1948**, *74*, 958. [[CrossRef](#)]
9. Levine, H.; Schwinger, J. On the Theory of Diffraction by an Aperture in an Infinite Plane Screen. II. *Phys. Rev.* **1949**, *75*, 1423. [[CrossRef](#)]
10. Kukhlevsky, S.V.; Mechler, M.; Samek, O.; Janssens, K. Analytical Model of the Enhanced Light Transmission Through Subwavelength Metal Slits: Green's function Formalism Versus Rayleigh's Expansion. *Appl. Phys. B Lasers Opt.* **2006**, *84*, 19–24. [[CrossRef](#)]
11. Kukhlevsky, S.V.; Mechler, M.; Csapo, L.; Janssens, K.; Samek, O. Enhanced Transmission Versus Localization of a Light Pulse by a Subwavelength Metal Slit. *Phys. Rev. B* **2004**, *70*, 195428. [[CrossRef](#)]
12. Neerhoff, F.L.; Mur, G. Diffraction of a plane electromagnetic wave by a slit in a thick screen placed between two different media. *Appl. Sci. Res.* **1973**, *28*, 73. [[CrossRef](#)]
13. Genet, C.; Ebbesen, T. Light in Tiny Holes. *Nature* **2007**, *445*, 390. [[CrossRef](#)] [[PubMed](#)]